Solid State Phenomena
ISSN: 1662-9779, Vol. 390, pp 63-74
doi:10.4028/p-4FOjpQ

Submitted: 2026-01-07
Revised: 2026-02-18
Accepted: 2026-02-21
Online: 2026-04-17

Deriving Macroscopic Damage Properties by Micromechanical Modeling of DP1000

Maximilian Neite[1,a*], Sebastian Münstermann[1,b]

[1]Institute of Metal Forming, RWTH Aachen University, Germany

[a*]maximilian.neite@ibf.rwth-aachen.de, [b]sebastian.muenstermann@ibf.rwth-aachen.de, (*corresponding author)

Keywords: Crystal Plasticity, Representative Volume Element, Micromechanical Modeling, Damage, Dual Phase Steel.

Abstract. Macroscopic damage models can describe the toughness behavior and formability of metals in terms of limit strains. However, it requires time-, cost-, and material-intensive calibration. In this work, a simulation framework is proposed to derive macroscopic damage model parameters and related properties directly from the microstructure. For this purpose, statistically Representative Volume Elements of the investigated DP1000 steel were generated utilizing the Python framework DRAGen. This was based on quantitative characterization of EBSD measurements of the present microstructure. Mechanical properties were assigned to the geometrical microstructure model by calibrating a phenomenological Crystal Plasticity model for distinct phases. Martensite cracking was identified as the predominant damage mechanism. This behavior on the microscale was represented by an isotropic brittle damage model in DAMASK, using a fracture mechanical literature value as the critical energy release rate parameter. The presented modeling approach enables stress state-dependent prediction of macroscopic damage properties out of the present microstructure.

Introduction

Dual Phase (DP) steel offers an excellent combination of high strength and good formability, which is why this class of Advanced High Strength Steels (AHSS) is highly attractive to the automotive industry [1,2]. It enables lightweight design in car body construction, one of the main challenges current car manufacturing faces [3]. Different types of DP steel can be achieved by tailoring the processing route, which results in different microstructures [4]. The produced microstructures provoke different macroscopic properties, like strength or damage tolerance, which are crucial for the design and manufacturing process [5,6]. This is part of the classical forward consideration of the process – microstructure – property relationship [7].

Macroscopic material properties, such as the toughness of steel, can be described using macroscopic damage models. These models also enable the prediction of forming limit curves, which are essential for assessing a material's formability [8]. However, applying these phenomenological models in practice is often limited by the significant experimental and numerical effort required to calibrate their parameters. The *Modified Bai-Wierzbicki* (MBW) damage model uses limit strains to separately describe ductile damage initiation and ductile failure based on the stress state, expressed by the Lode angle parameter and stress triaxiality. To cover a broad range of stress state conditions, various sample geometries are typically tested in experiments. Additionally, the effects of strain rate and temperature on material flow must be calibrated. [9,10]

For a backward, reverse engineering approach in microstructure design for tailored materials, it is essential to predict macroscopic material properties from the current microstructure directly [4,11]. To do this, micromechanical simulations of geometrical microstructure models can be conducted using Crystal Plasticity (CP) models [12]. Here, a Representative Volume Element (RVE) of the microstructure is often employed [13,14]. In the past, several RVE generators were developed to enhance accuracy by accounting for more microstructural features. The recently released Python framework *Discrete RVE Automation and Generation* (DRAGen) [15] can generate RVEs with banded structures, which are often necessary when studying DP steel [16,17]. Additionally, it creates input files for the simulation framework *Düsseldorf Advanced Material Simulation Kit* (DAMASK)

[18]. This framework allows for multi-physics CP simulations in a phase-field approach, incorporating mechanical, thermal, and damage effects simultaneously and interdependently.

The damage behavior in DP steels has been widely studied in recent years. Tasan et al. [4] reviewed experimental observations in the literature and summarized that damage typically initiates due to cracking of martensite, interface decohesion between ferritic and martensitic constituents, or a combination of both processes. These different damage mechanisms were observed to depend on microstructural characteristics, like phase fractions, ferrite grain size, or distribution and morphology of martensite. For DP steels with banded martensitic structures, martensite cracking was found to be the main damage initiation mechanism [19]. Also, numerical investigations were performed to study the damage behavior of DP steel micromechanically, considering both mechanisms [11,20–24] or specifically for the mechanism of interface decohesion [25,26] or martensite cracking [27].

In this paper, we present a workflow to derive macroscopic damage model parameters from the present microstructure. For this purpose, RVEs were generated with DRAGen based on a quantitative analysis of Electron Backscatter Diffraction (EBSD) measurements. The phenomenological CP model in DAMASK was calibrated to assign mechanical properties to the geometrical microstructure model. Finally, the isotropic brittle damage model implemented in DAMASK was applied to obtain stress state-dependent predictions of damage on the macroscale due to martensite cracking for a cold-rolled DP1000.

Microstructure Model

The ferritic-martensitic microstructure of DP1000 was investigated by EBSD measurements on a metallographically prepared sample of the Normal Direction (ND)-Transverse Direction (TD) plane. The captured area was about 100 x 100 mm² in size and measured with a step size of 50 nm. These EBSD data were evaluated quantitatively with the help of the software *OIM Analysis 2022 EDAX*. After the predefined Confidence Index standardization, grains were calculated based on a threshold angle of 5°, and grains smaller than five data points were excluded. Founded on the histogram of grain-average Image Quality, the ferritic and martensitic phases were distinguished. Through this separation, the phase ratios were determined by the number of data points per phase.

The grain morphology in the ferritic phase was described by fitted ellipses in terms of the lengths of major and minor semi-axes. Additionally, the grain's slope was expressed by the inclination angle between the ellipse's major axis and the horizontal axis of the EBSD image. Together with this geometrical description of the grains, their crystallographic orientation, defined by the Euler angles φ_1, ϕ, and φ_2, is stored in a *.csv* file.

A binary image of the EBSD measurements, colored by phase, was processed with functions of the *OpenCV* library in Python to describe the geometrical appearance of martensite quantitatively with ellipses. Large, band-like martensitic structures and smaller martensitic islands were analyzed individually. In this study, the focus is on larger microstructure volumes instead of a precise spatial resolution of fine hierarchical substructure constituents of the martensite, like laths or (sub-)blocks [28]. Those constituents were agglomerated to the quantitatively described martensite islands. The crystallographic orientation of martensitic constituents was not analyzed, since their orientation was later assumed to be random due to isotropic mechanical modeling of martensite.

The obtained results of the EBSD analysis are presented in Fig. 1 by Inverse Pole Figure (IPF) illustrations for the [001] direction. Ferritic grains of the investigated DP1000 steel exhibit an elongation along the TD. This observation is typical for so-called *pancake* grain morphology in cold-rolled materials, leading to the assumption that a similar elongation could be observed along the Rolling Direction (RD) in the RD-ND plane [29]. This results in an assumed grain morphology, where two ellipsoid's axes have a similar length, larger compared to the third ellipsoid's dimension. The second IPF depicts pixels assigned to the martensitic phase in black. From this, the phase fraction of martensite in the investigated DP1000 is determined to be about 28 %. Here, martensitic band-like formations in TD are visible, and are assumed to be spread in the RD-TD plane accordingly.

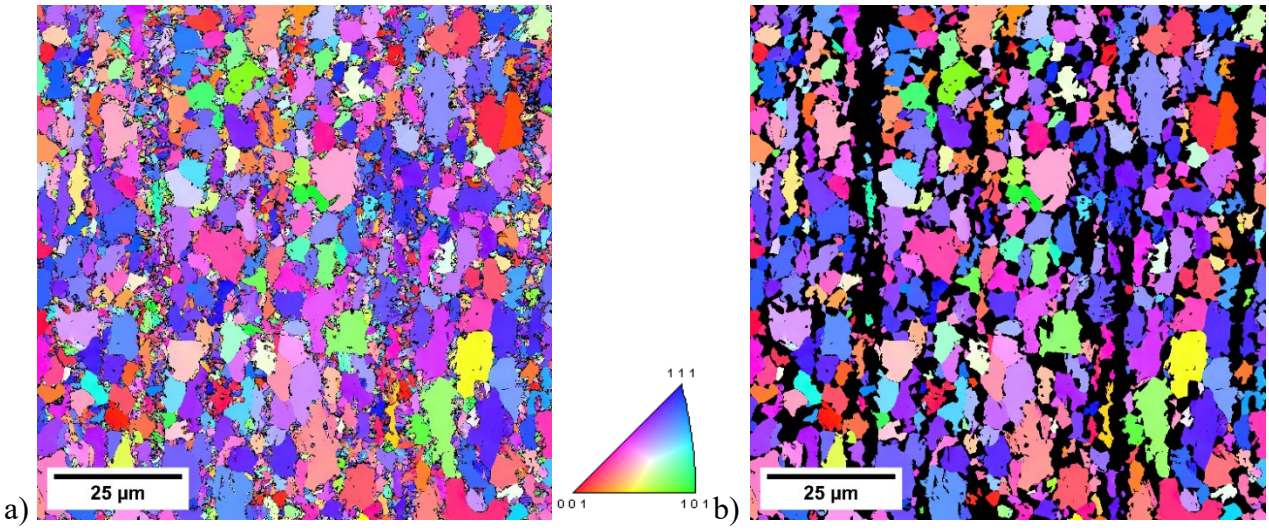

Fig. 1. EBSD analysis of investigated DP1000: a) IPF[001] for the ND-TD plane, and accordingly, in b) martensite is highlighted in black.

The gathered microstructure data were then used to train a synthetic input data generator for the following generation of RVEs. The trained generator is built on a *Wasserstein Generative Adversarial Network with Gradient Penalty* (WGAN-GP) [30]. It is capable of reproducing the statistical distribution as well as interdependencies of parameters, which quantitatively describe the investigated microstructure.

Afterwards, three-dimensional RVEs were generated utilizing DRAGen. Here, the synthetic microstructural data produced by the trained WGAN-GP were used as input to create ellipsoids depicting grains within the discretized volume element. For this work, ten statistically equivalent RVEs of the investigated DP1000 steel were generated. Each one has an edge length of 50 µm with a resolution of 1.28, resulting in RVEs containing 64 x 64 x 64 voxels. One martensite band was inserted into each RVE, following the aforementioned quantitative microstructure characterization of the investigated material.

As an example, one generated RVE of DP1000 is depicted in Fig. 2, showing the grains in individual colors and the martensitic band horizontally in red.

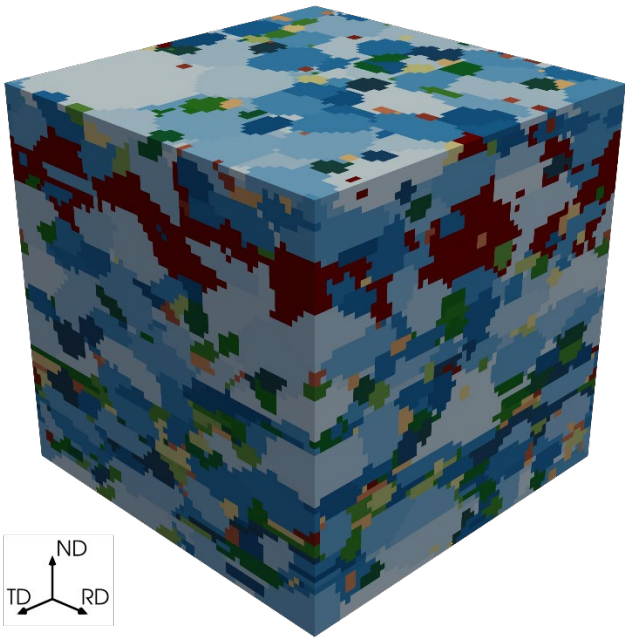

Fig. 2. Exemplary RVE of the DP1000 generated with DRAGen, color-coded by grains.

Here, the assumed *pancake* morphology of the ferrite grains can be observed as well. Most of the generated RVEs contain a martensite phase fraction of around 30 %, which is higher compared to the experimental findings. This inaccuracy is caused by the algorithm implemented in DRAGen to create banded structures, making it more difficult to reach the targeted phase ratios during RVE generation.

Crystal Plasticity

DAMASK was used in this study to assign mechanical properties to the geometrical microstructure model by employing a phenomenological CP model (*phenopowerlaw*) for ferrite and the *isotropic* CP model for martensite [18]. The model for ferrite relies on anisotropic dislocation reactions and shearing in specifically activated slip systems, whereas the mechanical behavior of martensite was modeled to be direction independent. However, this model depicts not only the elastic mechanical behavior of martensite. Its hardening law, defined by the hardening exponent a and the initial hardening factor h_0, allows the evolution of the resistance to plastic deformation from an initial ξ_0 to a saturated value ξ_∞, analogous to the model used for ferrite. Both models obey a rate dependency implemented as a power-law relationship with the reference shear rate $\dot{\gamma}_0$ and the rate sensitivity n.

The CP parameter sets for both phases were calibrated separately in this study based on an inverse procedure. The CP parameters were adjusted iteratively to match the macroscopic flow behavior of the investigated DP1000, studied in a previous work [31]. The literature suggests more sophisticated calibration procedures involving micropillar compression tests [32] or nanoindentations [13]. Noteworthy, these approaches also require considerable experimental effort.

Empirical correlations from literature connecting local chemical composition with flow behavior were used to determine a solely martensitic flow curve. This approach [33] defines the flow properties of martensitic microstructures as a composition of Peierls stress, strengthening due to carbon located at interstitial lattice positions, and strengthening due to dislocation effects. Segregation of alloying elements arising from partitioning and restricted solubility leads to distinct chemical compositions of ferrite and martensite. In previous studies [13], it was observed that particularly manganese and carbon accumulate within the martensitic phase of a DP steel. To characterize these local variations in chemical composition, specifically carbon and manganese content, multiple line scans of Electron Probe Microanalysis (EPMA) were performed over the microstructure investigated. Also, the global chemical composition of homogenously distributed alloying elements defining the material's strength was examined with the help of Optical Emission Spectroscopy (OES). Flow curve partitioning, according to the determined phase fractions, was applied to obtain an individual curve for ferrite [34]. The phases' flow curves, calculated based on chemistry and flow curve partitioning, and the experimental (total) flow curve of the DP1000 are represented in Fig. 3 as dashed lines.

An RVE comprised of only one martensite grain was loaded with quasi-static, uniaxial tension, and the homogenized values of equivalent stress over plastic equivalent strain were extracted. The curve was compared to the martensitic flow curve obtained from the local chemistry, and the CP parameter set for martensite was adjusted until both curves were in good approximation. Afterwards, the ten generated RVEs of DP1000 were subjected to the same loading condition as the martensitic RVE to define the CP parameter set for ferrite in a way that the calculated ferritic flow curve is represented.

The resulting curves from the RVE simulations are depicted in Fig. 3. The overall mechanical responses of the RVEs indicate higher equivalent stresses compared to the experimental flow curve, regardless of the observed scatter. This can be explained by the higher amount of martensite within the created RVEs in relation to the experimentally determined phase fraction. In general, both calibrated CP parameter sets describe the mechanical behavior of the individual phases well, especially at larger strains. The deflections in hardening behavior at small strains can be neglected because of the study's focus on the prediction of ductile damage at usually elevated strains. This results in a sufficient representation of the mechanical properties of DP1000 in micromechanical simulations utilizing the generated RVEs and the calibrated CP models. Table 1 concludes the calibrated values for the important CP parameters governing plastic material behavior.

Table 1. Calibrated CP parameter sets of martensite and ferrite to represent the mechanical behavior of DP1000.

	$\dot{\gamma}_0$ (s^{-1})	n (−)	ξ_0 (MPa)	h_0 (MPa)	ξ_∞ (MPa)	a (−)
Martensite	0.001	100	685	1000	685	1.0
Ferrite	0.001	100	210	1000	520	2.0

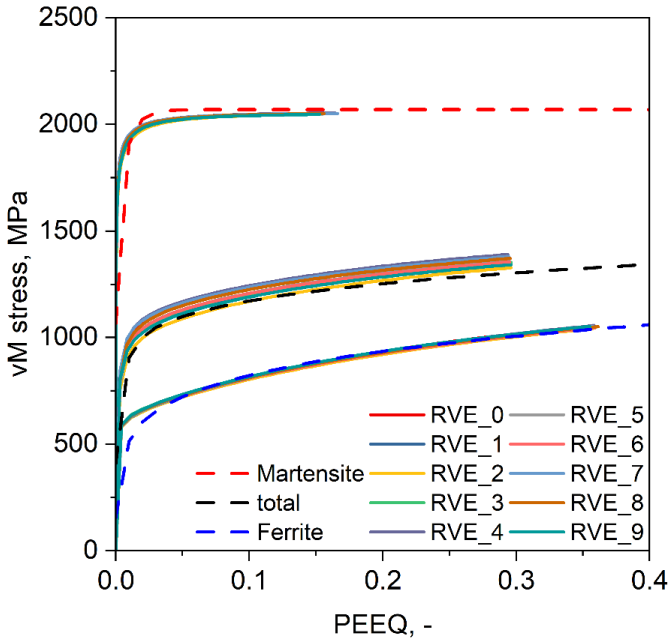

Fig. 3. Results of the CP Calibration in terms of equivalent stress over plastic equivalent strain curves of ten simulated RVEs; comparison with reference (dashed) curves for ferrite and martensite phases, as well as the overall experimental (total) curve.

Damage Modeling

Scanning Electron Microscopy (SEM) was used to study the damage mechanism of the investigated DP1000 on the microscale. For this purpose, macroscopically tested samples from a previous study [31] were metallographically prepared in the vicinity of the fracture surface. Martensite cracking was determined as the predominant damage mechanism for distinct stress states at quasi-static conditions. Additionally, only a small number of pores were observed near the fracture surfaces of the ex-situ investigated samples, indicating rapid ductile damage evolution in DP1000.

In this work, martensite cracking was modeled micromechanically within the DAMASK framework [18]. Its phase field approach contains implemented damage models to describe damage initiation and evolution non-locally. The damage field variable φ can vary from an undamaged ($\varphi = 1$) to a fully damaged ($\varphi = 0$) condition. A sharp crack is assumed as a diffuse crack interface with gradually degrading material properties by introducing a length scale parameter l_c. The spectral solver, based on the Fast Fourier Transform (FFT) method, numerically solves the following differential equation describing damage evolution

$$\mu_\varphi \dot{\varphi} = f_\varphi - \mathrm{Div}\,\mathbf{f}_\varphi. \tag{1}$$

Here, damage viscosity is represented by μ_φ, damage driving force by f_φ and damage flux by $\mathbf{f}_\varphi$. Following Griffith's criterion, brittle damage is created when sufficient energy required to build new internal surfaces, related to the surface tension G, is provided by the release of stored elastic energy. So, the damage flux is defined as

$$\mathbf{f}_\varphi = -G\, l_c\, \nabla\varphi \tag{2}$$

and the damage driving force, derived by minimization of the total free energy density, as

$$f_\varphi = \frac{G}{l_c} - \varphi \boldsymbol{S}:\boldsymbol{E}. \tag{3}$$

In this model, the damage influence on the stored elastic energy is implemented by a modified Hooke's law, with $\boldsymbol{S}$ being the second Piola-Kirchhoff stress tensor, $\boldsymbol{E}$ the elastic Green-Lagrange strain tensor, and $\boldsymbol{C}$ the elastic stiffness tensor

$$\boldsymbol{S} = \varphi^2 \boldsymbol{C}:\boldsymbol{E}. \tag{4}$$

In this study, the *isobrittle* damage model [35] implemented in DAMASK was applied to model damage in martensite. For this purpose, $\mu_\varphi = 0.001$ and $l_c = 2$ µm was set. The governing model parameter, critical surface energy, G_c was defined as $423\ \mathrm{J\ m^{-2}}$. This value was approximated from literature [36], which reveals the mean fracture toughness of martensite in DP800 with microcantilever bending tests to $J_{i,2\%} = 423\ \mathrm{J\ m^{-2}}$. This value was adopted and approximated as a characteristic energy-equivalent damage parameter for martensite in the RVE simulations of this study, because high experimental effort is required, and more precise data for DP1000 are not available.

Damage initiation in martensite was assumed in the micromechanical simulations as soon as any material point assigned to the martensite phase leaves the undamaged state. Typically, multiple material points reach the damaged state simultaneously within an increment, leading to numerical instabilities and subsequent loss of convergence under the default solver settings. A detailed study of crack propagation through the 3D RVE would therefore require significantly increased computational resources. At this instant, where $\varphi < 1$, homogenized values in terms of average values over all material points containing the RVE were calculated for plastic equivalent strain ε^p, stress triaxiality η, and Lode angle parameter $\bar{\theta}$. By doing this homogenization, the results obtained with periodic RVEs in virtual experiments were bridged to macroscopic properties. This way, each RVE simulation results in one data point in the ε^p-η- $\bar{\theta}$-space representing damage initiation in martensite on the macroscale.

Distinct prescribed deformation gradient rates were applied to each RVE to obtain stress state-dependent results. Quasi-static conditions were simulated for Uniaxial, Plane Strain (PS), Equi-Biaxial (Biaxial), and Non-Equi-Biaxial (NE-Biaxial) tension. Those loading conditions are illustrated in Fig. 4, which shows a deformed RVE for each stress state, together with the reference cubic geometry of the RVE as a black wireframe. The deformed RVEs are colored by equivalent stress (vM stress) values to indicate the stress distribution. Regardless of the stress state, a big range in stress values can be observed due to the distinct phases of ferrite and martensite. Martensite shows significantly higher and uniform stress values due to the flat stress-strain curve without hardening, set during CP calibration (cf. Fig. 3). Since the calibrated CP parameter set of the ferritic phase allows for strain hardening, the stress distribution follows the most favorable grain orientations for dislocation slip. These favorable orientations depend on the direction of loading and thus the stress state.

The ten generated RVEs of DP1000 were subjected to each prescribed stress state to consider the scatter of damage. The mean damage initiation strain and its standard deviation obtained from these micromechanical simulations were calculated per stress state. In Fig. 5, the resulting data points are compared to the macroscopically and experimentally-numerically calibrated MBW damage locus of the investigated DP1000 derived in a previous study [31]. This ductile failure locus is assumed to be $\bar{\theta}$-symmetric and can be mathematically described with $D_1 = 0.12$, $D_2 = 0.12$, $D_3 = 0.18$, and $D_4 = 1.52$ by

$$\varepsilon^p(\eta, \bar{\theta}) = (D_1 e^{-D_2\eta} - D_3 e^{-D_4\eta})\bar{\theta}^2 + D_3 e^{-D_4\eta}. \tag{5}$$

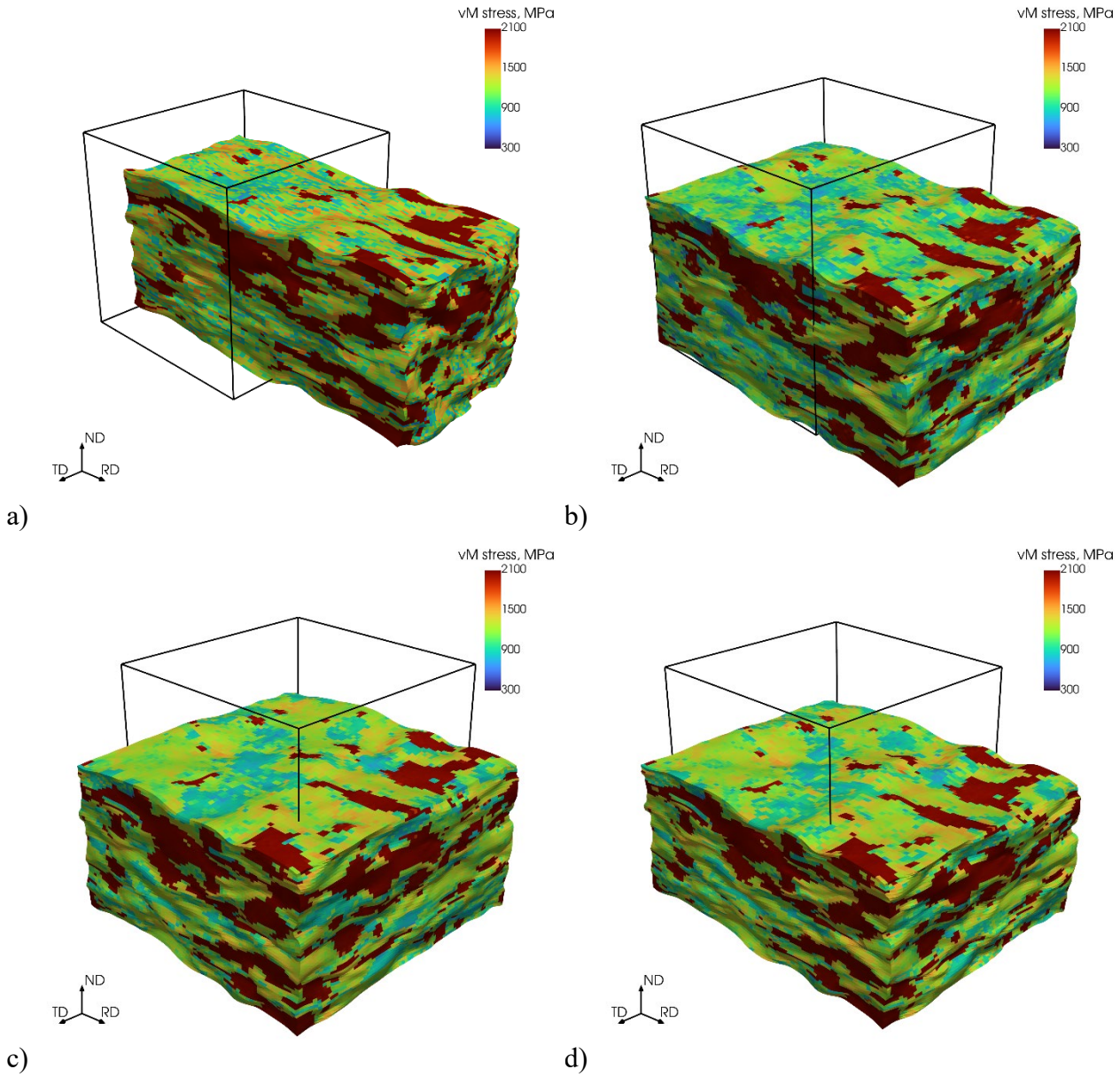

Fig. 4. Simulation of an RVE under different stress states due to distinct boundary conditions: a) uniaxial, b) plane strain, c) equi-biaxial, and d) non-equi biaxial; the black wireframe shows initial cubic RVE geometry, and the distribution of equivalent stress (vM stress) is illustrated by color code.

Overall, the micromechanically derived data points are located in the vicinity of the conventionally calibrated MBW damage locus. Here, a macroscopic MBW ductile failure locus is compared to derived data points representing ductile damage initiation in martensite. This can be justified, since damage on the macroscopic scale was modeled in an uncoupled manner due to the observed material behavior. Additionally, the results of the SEM investigations have shown rapid damage evolution in the investigated DP1000, resulting in prompt ductile failure after damage initiation. At the edges of the illustrated $\bar{\theta}$-range, specifically uniaxial and biaxial stress states, the predicted damage strain is closer to the reference MBW locus compared to predictions at $\bar{\theta}$ around 0. Even though the reference values on the MBW locus are located slightly outside the standard deviation range of the predicted damage strains for most stress states, the results demonstrate the capability of the presented simulation framework. The reference MBW locus is obtained by fitting the locus to multiple macroscopically determined supporting points. Therefore, even the reference locus can contain small deflections at certain stress states. Further, approximations were made when adopting an experimental value of a

DP800 as the governing CP model parameter G_c for DP1000. Noteworthy, in both cases, martensite cracking was described and investigated. In this study, the robustness of the simulation framework to predict macroscopic damage properties was evaluated by simulating multiple statistically equivalent RVEs. However, sensitivity studies on the influence of the key CP model parameter G_c could also be incorporated in the future to demonstrate the model's capabilities and quantify its predictive limits. For DP steels exhibiting a damage mechanism other than martensite cracking, the suitability of the applied model is questionable and needs to be investigated. Finally, inaccuracies created in the microstructure model during RVE generation and following CP calibration are propagated and influence the predictions.

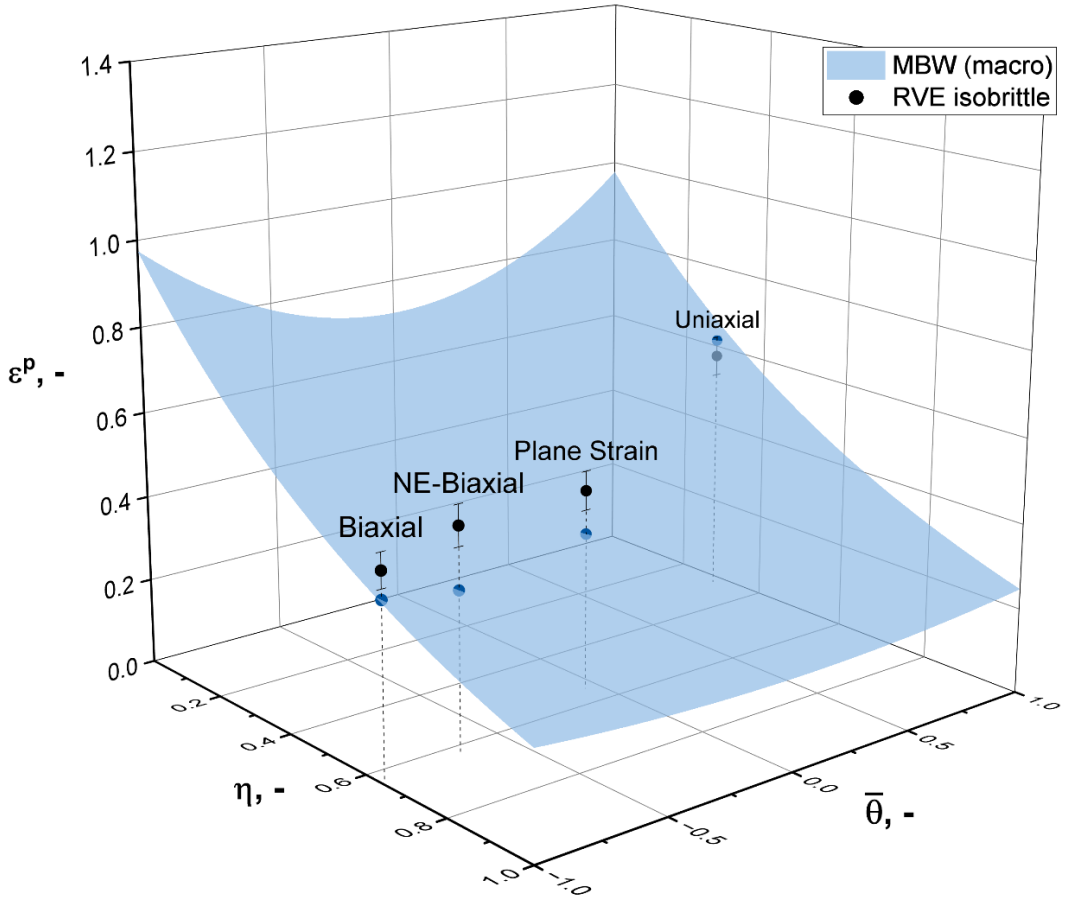

Fig. 5.Plastic equivalent strains for damage and their standard deviations derived by RVE simulations compared with the macroscopic MBW locus in dependence on the stress state.

Summary

This work presents a simulation framework to micromechanically derive macroscopic damage properties directly from the present microstructure. To do so, RVEs were generated utilizing DRAGen based on quantitative data gathered from EBSD measurements on DP1000 steel. The chemical composition was captured to empirically calculate individual flow curves for ferrite and martensite. CP parameter sets of a phenomenological CP model implemented in DAMASK were calibrated by inverse, iterative fitting to the flow curves for both phases. The generated RVEs contain more martensite than targeted, hence the total flow curves of CP simulations are slightly above the experimental one. The *isobrittle* damage model implemented in DAMASK was employed to micromechanically model martensite cracking, which was observed by SEM as the predominant damage mechanism in the investigated material. An experimentally measured toughness of martensite was adopted from literature as the model's governing parameter, the critical surface energy G_c. Ten RVEs were micromechanically simulated under distinct prescribed loading conditions to account for

scatter and the stress state dependency. The procedure was performed on a DP1000 steel and validated with existing macroscopically examined damage properties of this material. The predicted damage strains are close to the reference damage locus described by the MBW model. Considering the assumptions made for the G_c parameter and the deviations resulting from small inaccuracies during RVE generation and consecutive CP calibration, the proposed simulation framework is capable of predicting damage properties of DP1000 from its microstructure in good approximation. The resource-efficient way of determining macroscopic damage properties can also be used in the future for reverse engineering in material design to optimize microstructures.

Further studies are planned to validate the results based on macroscopic simulations using the micromechanically calibrated damage parameters of the MBW model. Additionally, studies on the subsequent damage evolution within the RVE after damage initiation or on incorporating multiple damage mechanisms simultaneously in micromechanical simulations could give further insights into the damage behavior, meaningful for optimizing materials by tailoring resistance microstructures.

Acknowledgements

This work was funded by the Deutsche Forschungsgemeinschaft (DFG, German Research Foundation) – Project number 391544620. Simulations were performed with computing resources granted by RWTH Aachen University under project rwth1670. The authors gratefully acknowledge material supply from SSAB AB.

References

[1] R. Kuziak, R. Kawalla, S. Waengler, Advanced high strength steels for automotive industry, Archives of Civil and Mechanical Engineering 8 (2008) 103–117. https://doi.org/10.1016/S1644-9665(12)60197-6.

[2] N. Baluch, Z.M. Udin, C.S. Abdullah, Advanced High Strength Steel in Auto Industry: an Overview, Eng. Technol. Appl. Sci. Res. 4 (2014) 686–689. https://doi.org/10.48084/etasr.444.

[3] C.D. Horvath, Advanced steels for lightweight automotive structures, in: P.K. Mallick (Ed.), Materials, design and manufacturing for lightweight vehicles, Second edition, Woodhead Publishing an imprint of Elsevier, Oxford, 2021, pp. 39–95.

[4] C.C. Tasan, M. Diehl, D. Yan, M. Bechtold, F. Roters, L. Schemmann, C. Zheng, N. Peranio, D. Ponge, M. Koyama, K. Tsuzaki, D. Raabe, An Overview of Dual-Phase Steels: Advances in Microstructure-Oriented Processing and Micromechanically Guided Design, Annu. Rev. Mater. Res. 45 (2015) 391–431. https://doi.org/10.1146/annurev-matsci-070214-021103.

[5] K. Park, M. Nishiyama, N. Nakada, T. Tsuchiyama, S. Takaki, Effect of the martensite distribution on the strain hardening and ductile fracture behaviors in dual-phase steel, Materials Science and Engineering: A 604 (2014) 135–141. https://doi.org/10.1016/j.msea.2014.02.058.

[6] M.T. Kim, T.M. Park, K.-H. Baik, W.S. Choi, J. Han, Effects of cold rolling reduction ratio on microstructures and tensile properties of intercritically annealed medium-Mn steels, Materials Science and Engineering: A 752 (2019) 43–54. https://doi.org/10.1016/j.msea.2019.02.091.

[7] E. Evin, J. Kepič, K. Buriková, M. Tomáš, The Prediction of the Mechanical Properties for Dual-Phase High Strength Steel Grades Based on Microstructure Characteristics, Metals 8 (2018) 242. https://doi.org/10.3390/met8040242.

[8] M. Müller, N. Fehlemann, T. Herrig, D. Lenz, M. Könemann, T. Bergs, S. Münstermann, Forming Limit of Dual Phase Steel: An Experimental and Numerical Investigation, in: K. Mocellin, P.-O. Bouchard, R. Bigot, T. Balan (Eds.), Proceedings of the 14th International Conference on the Technology of Plasticity - Current Trends in the Technology of Plasticity: ICTP 2023 - Volume 2, firstst ed. twentiethtwenty-fourth, Springer Nature Switzerland; Imprint Springer, Cham, 2024, pp. 184–193.

[9] B. Wu, X. Li, Y. Di, V. Brinnel, J. Lian, S. Münstermann, Extension of the modified Bai-Wierzbicki model for predicting ductile fracture under complex loading conditions, Fatigue Fract Eng Mat Struct 40 (2017) 2152–2168. https://doi.org/10.1111/ffe.12645.

[10] J. Lian, M. Sharaf, F. Archie, S. Münstermann, A hybrid approach for modelling of plasticity and failure behaviour of advanced high-strength steel sheets, International Journal of Damage Mechanics 22 (2013) 188–218. https://doi.org/10.1177/1056789512439319.

[11] N. Kusampudi, M. Diehl, Inverse design of dual-phase steel microstructures using generative machine learning model and Bayesian optimization, International Journal of Plasticity 171 (2023) 103776. https://doi.org/10.1016/j.ijplas.2023.103776.

[12] M. Diehl, M. Groeber, C. Haase, D.A. Molodov, F. Roters, D. Raabe, Identifying Structure–Property Relationships Through DREAM.3D Representative Volume Elements and DAMASK Crystal Plasticity Simulations: An Integrated Computational Materials Engineering Approach, JOM 69 (2017) 848–855. https://doi.org/10.1007/s11837-017-2303-0.

[13] N. Vajragupta, P. Wechsuwanmanee, J. Lian, M. Sharaf, S. Münstermann, A. Ma, A. Hartmaier, W. Bleck, The modeling scheme to evaluate the influence of microstructure features on microcrack formation of DP-steel: The artificial microstructure model and its application to predict the strain hardening behavior, Computational Materials Science 94 (2014) 198–213. https://doi.org/10.1016/j.commatsci.2014.04.011.

[14] S. Bargmann, B. Klusemann, J. Markmann, J.E. Schnabel, K. Schneider, C. Soyarslan, J. Wilmers, Generation of 3D representative volume elements for heterogeneous materials: A review, Progress in Materials Science 96 (2018) 322–384. https://doi.org/10.1016/j.pmatsci.2018.02.003.

[15] M. Henrich, N. Fehlemann, F. Bexter, M. Neite, L. Kong, F. Shen, M.J. Könemann, M. Dölz, S. Münstermann, DRAGen - A deep learning supported RVE generator framework for complex microstructure models, Heliyon 9 (2023) e19003. https://doi.org/10.1016/j.heliyon.2023.e19003.

[16] C.C. Tasan, J. Hoefnagels, M. Geers, Microstructural banding effects clarified through micrographic digital image correlation, Scripta Materialia 62 (2010) 835–838. https://doi.org/10.1016/j.scriptamat.2010.02.014.

[17] N. Fehlemann, A.L. Suarez Aguilera, S. Sandfeld, F. Bexter, M. Neite, D. Lenz, M. Könemann, S. Münstermann, 2023. Identification of Martensite Bands in Dual-Phase Steels: A Deep Learning Object Detection Approach Using Faster Region-Based-Convolutional Neural Network. steel research int. 94, 2200836. https://doi.org/10.1002/srin.202200836.

[18] F. Roters, M. Diehl, P. Shanthraj, P. Eisenlohr, C. Reuber, S.L. Wong, T. Maiti, A. Ebrahimi, T. Hochrainer, H.-O. Fabritius, S.D. Nikolov, M. Friák, N. Fujita, N. Grilli, K.G. Janssens, N. Jia, P.J. Kok, D. Ma, F. Meier, E. Werner, M. Stricker, D.M. Weygand, D. Raabe, DAMASK – The Düsseldorf Advanced Material Simulation Kit for modeling multi-physics crystal plasticity, thermal, and damage phenomena from the single crystal up to the component scale, Computational Materials Science 158 (2019) 420–478. https://doi.org/10.1016/j.commatsci.2018.04.030.

[19] G. Avramovic-Cingara, Y. Ososkov, M.K. Jain, D.S. Wilkinson, Effect of martensite distribution on damage behaviour in DP600 dual phase steels, Materials Science and Engineering: A 516 (2009) 7–16. https://doi.org/10.1016/j.msea.2009.03.055.

[20] E.E. Aşık, E.S. Perdahcıoğlu, T. van den Boogaard, An RVE-Based Study of the Effect of Martensite Banding on Damage Evolution in Dual Phase Steels, Materials (Basel) 13 (2020). https://doi.org/10.3390/ma13071795.

[21] C. Tian, C.F. Kusche, A. Medina, S. Lee, M.A. Wollenweber, R. Pippan, S. Korte-Kerzel, C. Kirchlechner, Understanding the damage initiation and growth mechanisms of two DP800 dual phase grades, Materials & Design 238 (2024) 112630. https://doi.org/10.1016/j.matdes.2024.112630.

[22] Q. Lai, O. Bouaziz, M. Gouné, L. Brassart, M. Verdier, G. Parry, A. Perlade, Y. Bréchet, T. Pardoen, Damage and fracture of dual-phase steels: Influence of martensite volume fraction, Materials Science and Engineering: A 646 (2015) 322–331. https://doi.org/10.1016/j.msea.2015.08.073.

[23] C.C. Tasan, J. Hoefnagels, M. Diehl, D. Yan, F. Roters, D. Raabe, Strain localization and damage in dual phase steels investigated by coupled in-situ deformation experiments and crystal plasticity simulations, International Journal of Plasticity 63 (2014) 198–210. https://doi.org/10.1016/j.ijplas.2014.06.004.

[24] T. de Geus, R. Peerlings, M. Geers, Competing damage mechanisms in a two-phase microstructure: How microstructure and loading conditions determine the onset of fracture, International Journal of Solids and Structures 97-98 (2016) 687–698. https://doi.org/10.1016/j.ijsolstr.2016.03.029.

[25] I.U. Aydiner, B. Tatli, T. Yalçinkaya, Investigation of failure mechanisms in dual-phase steels through cohesive zone modeling and crystal plasticity frameworks, International Journal of Plasticity 174 (2024) 103898. https://doi.org/10.1016/j.ijplas.2024.103898.

[26] L. Liu, F. Maresca, T. Vermeij, J. Hoefnagels, M. Geers, V.G. Kouznetsova, An integrated experimental-numerical study of martensite/ferrite interface damage initiation in dual-phase steels, Scripta Materialia 239 (2024) 115798. https://doi.org/10.1016/j.scriptamat.2023.115798.

[27] A. Ramazani, Y. Chang, U. Prahl, Characterization and Modeling of Failure Initiation in Bainite-Aided DP Steel, Adv Eng Mater 16 (2014) 1370–1380. https://doi.org/10.1002/adem.201300556.

[28] F.-J. Gallardo-Basile, Y. Naunheim, F. Roters, M. Diehl, Lath Martensite Microstructure Modeling: A High-Resolution Crystal Plasticity Simulation Study, Materials (Basel) 14 (2021). https://doi.org/10.3390/ma14030691.

[29] N.C. Fehlemann, I. Biermann, S. Münstermann, Exploring structure–property relations in dual phase steels using crystal plasticity and variance based global sensitivity analysis, Materials & Design 259 (2025) 114794. https://doi.org/10.1016/j.matdes.2025.114794.

[30] F. Pütz, M. Henrich, N. Fehlemann, A. Roth, S. Münstermann, Generating Input Data for Microstructure Modelling: A Deep Learning Approach Using Generative Adversarial Networks, Materials (Basel) 13 (2020). https://doi.org/10.3390/ma13194236.

[31] C. Zeng, X. Fang, Specimen geometry design for plasticity and fracture characterization of sheet metal under high testing speed and various stress states, Thin-Walled Structures 186 (2023) 110688. https://doi.org/10.1016/j.tws.2023.110688.

[32] N.C. Fehlemann, A. Medina, S. Lee, C. Kirchlechner, S. Münstermann, Crystal plasticity parameter identification via statistical relevant micropillar compression, Acta Materialia 297 (2025) 121321. https://doi.org/10.1016/j.actamat.2025.121321.

[33] R.-M. Rodriguez, I. Gutiérrez, Unified Formulation to Predict the Tensile Curves of Steels with Different Microstructures, MSF 426-432 (2003) 4525–4530. https://doi.org/10.4028/www.scientific.net/MSF.426-432.4525.

[34] I. Gutiérrez, Ame Modelling the Mechanical Behaviour of Steels with Mixed Microstructures, J. Metall. Mater. Eng 11 (2005) 201–214.

[35] M. Diehl, M. Wicke, P. Shanthraj, F. Roters, A. Brueckner-Foit, D. Raabe, Coupled Crystal Plasticity–Phase Field Fracture Simulation Study on Damage Evolution Around a Void: Pore Shape Versus Crystallographic Orientation, JOM 69 (2017) 872–878. https://doi.org/10.1007/s11837-017-2308-8.

[36] C. Tian, C. Kirchlechner, The fracture toughness of martensite islands in dual-phase DP800 steel, Journal of Materials Research 36(2021) 2495-2504.https://doi.org/10.1557/s43578-021-00150-4.

The publication of this article was funded by the RWTH Aachen University 10.13039/501100007210